A new approach of robust speed-sensorless control of doubly fed induction motor fed by photovoltaic solar panel

Mekki Mounira[1], Cherifi Djamila[2]
[1]Department of Electrical Engineering, Faculty of Sciences and Applied Sciences, Larbi Ben M'hidi University, Oum El Bouaghi, Algeria
[2]Department of Electrical Engineering, Faculty of Technology, Tahar Moulay University, Saida, Algeria

Article Info

Article history:

Received Jan 11, 2022
Revised Sep 15, 2022
Accepted Sep 29, 2022

Keywords:

Double-fed induction motor
MPPT
Photovoltaic solar panel
Sensorless control
Sliding mode observer
Vector control

ABSTRACT

In this work, we presented the modelling and simulation of the electrical operation of a photovoltaic (PV) system adapted by an MPPT control, the latter is applied to the robust observer for the control of the speed without sensor of a double fed induction motor (DFIM).Our machine is powered by the PV system, where the chosen control is the direct field oriented control with sliding mode speed regulator is used for the control of this machine which is powered by two pulse-width modulation (PWM) voltage inverters, finally the speed estimation of induction motor with observer based dual feed in sliding mode is presented. The simulation results show the efficiency of the proposed method.

Corresponding Author:

Mekki Mounira
Department of Electrical Engineering, Faculty of Sciences and Applied Sciences
Larbi Ben M'hidi University
Oum El Bouaghi, Algeria
Email: mouniramekki9@gmail.com

1. INTRODUCTION

Renewable energies are environmentally friendly energies, among the advantages, they are not polluting, non-CO_2 waste, they fight against the greenhouse, and help create new jobs. Photovoltaic energy is the most significant energy in renewable energy which has been attracting growing interest in recent years. Today photovoltaic (PV) technologies are sufficiently mature and measured to take a real take-off in the field of power applications. The basic elements are cells that convert solar radiation into current electricity (photovoltaic effect) the creation and optimization of photovoltaic systems are the current problems, the resolution of these problems surely leads to a better use of solar energy [1]–[5].

The doubly fed induction motor (DFIM) is the most popular due to its high performance, energy quality [6]–[8]. However, this machine presents difficulties at the level of its control because this one presents a nonlinear system, strongly coupled, with fast dynamics and with parameters varying in time [9]–[11]. The flux-oriented vector control was developed to control the torque in transient conditions [12]–[15].

The control of the speed and/or the position of the rotor requires the presence of an incremental encoder (a sensor). However, this sensor must be set up in its environment of use and additional space for its installation. In addition, the introduction of this fragile device results in a decrease in the reliability of the system which requires special care for itself. has become a serious subject of research study in recent years [16]–[18]. This work will be devoted to the implementation of an algorithm for observing the speed of a DFIM using the sliding mode observer.

The control laws using conventional regulators give good performance in the case of systems with constant parameters, but for systems with variable structures, the sliding mode regulator is used [19]–[21]. In this work we are interested in the three-level inverter with nuclear pore complex (NPC) structure [22], [23]. This work concerns sensorless speed and flux control equipped with robust speed regulator for doubly fed induction motor fed by maximum power point tracking (MPPT) photovoltaic generator.

2. SYSTEM DESCRIPTION

The proposed control structure is indicated by Figure 1. This structure comprises the following elements: a photovoltaic generator, a boost converter (DC-DC), and a three-level inverter which supplies the machine. The DC-DC converter permanently extracts the maximum power of the PV module ensuring at the same time a good performance coping with power changes introduced by the change in the environmental conditions.

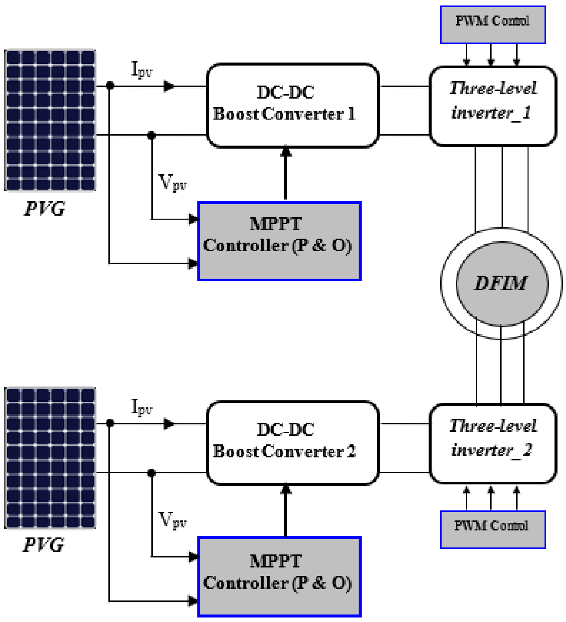

Figure 1. Block diagram of the full system

3. MATHEMATICAL MODEL FOR A PHOTOVOLTAIC MODULE

The solar cells are the main elements that make up the photovoltaic panel shown in Figure 2. Other modules are added according to the requested power. The current I(V) as illustrated in (1) [24]–[26].

$$\left\{ I_{\mathrm{pv}} = N_p I_{ph} - N_p I_s \left\{ e\left[\frac{q(V_{pv}+R_S I_{pv})}{N_S AKT}\right] - 1 \right\} - N_p \frac{q(V_{pv}+R_S I_{pv})}{R_p N_S} \right. \tag{1}$$

The photocurrent I_{ph} is given by (2):

$$I_{ph} = [I_s + k_i(T - T_r)]\frac{S}{100} \tag{2}$$

where

$$I_s = I_{so} * \left(\frac{T}{T_r}\right)^3 * e\left[\left(-\frac{q.E_g}{A.K}\right) * \left(\frac{1}{T_r} - \frac{1}{T}\right)\right] \tag{3}$$

and

$$A = \frac{q(V_{pv}+R_S I_{pv})}{N_S} \tag{4}$$

Table 1 summarizes the electrical characteristics of the PV module supplied by the manufacturer BP3160. We used some data, and applied it in the simulation model. The Simulink model of PV module is presented in Figure 3. A photovoltaic cell is defined by its electrical characteristic curves (current voltage) and (power-voltage) [27], [28]. Until the open circuit, as indicated by the characteristic I (V) in Figure 4(a). Whenever the voltage increases, the current has a constant value which is equal to: 4.8 A, then arrived at a certain value the current drops from 4.8 A to 0 A and the characteristic P (V) in Figure 4(b). Each time the voltage increases, the power increases and then arrived at a certain value which is V = 35 V, the power drops.

– Variation of irradiation

The I(V) and P(V) characteristics of the PV generator obtained for different values of irradiation under a constant temperature shown in Figure 5. These curves show that the output power of the solar panels is directly proportional to the irradiance, lower irradiation results in reduced output power of the PV array. However, only the output current is significantly affected by the irradiation while the voltage V_{OC} varies only very little and the change is considered negligible, because under the working principle of the solar cell, the current is proportional to the flux of photons [29], [30].

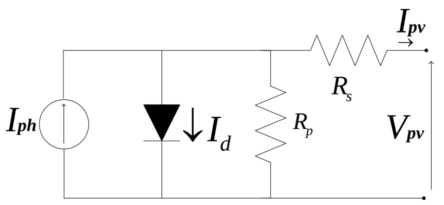

Figure 2. Equivalent circuit of PV cell

Table 1. Specifications of PV module BP 3160

Characteristics	Values
Typical peak power	160 W
Voltage at peak power	34.5 V
Current at peak power	4.55 A
Short-circuit current (I_{SC})	4.8 A
Open- circuit voltage (V_{OC}	44.2 V
Temperature coefficient of $I_{SC}(k_1)$	(0.065±0.015) %K
Temperature coefficient of V_{OC} (k_2)	(160±20) mV/K
Temperature coefficient of power	-(0.5±0.05) %K
Factor of PV technology(a)	1.5
Serie resistance (R_S)	5 mΩ

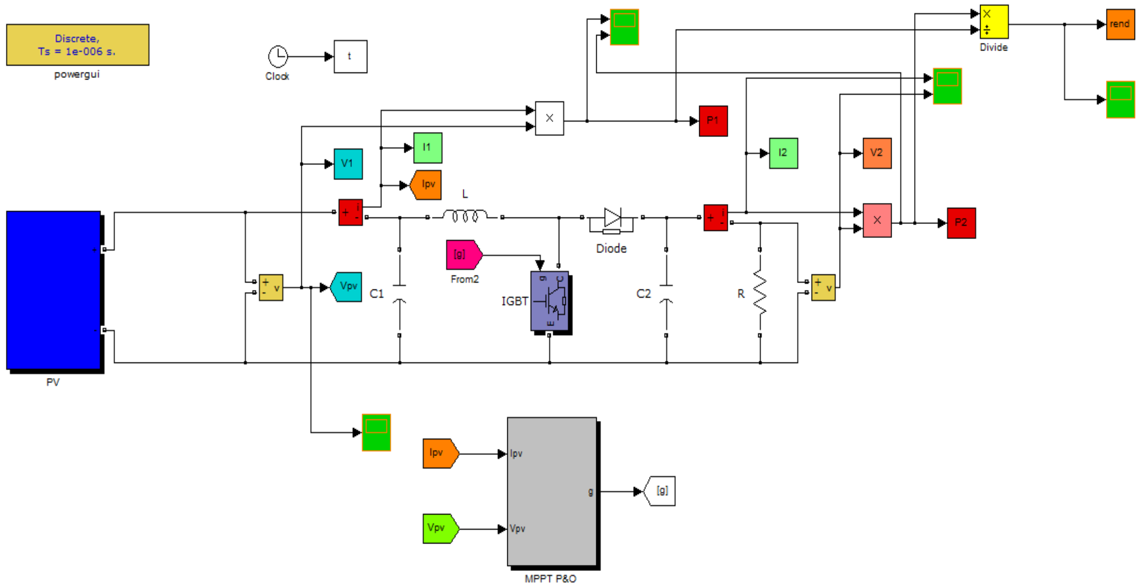

Figure 3. Simulink model of PV module

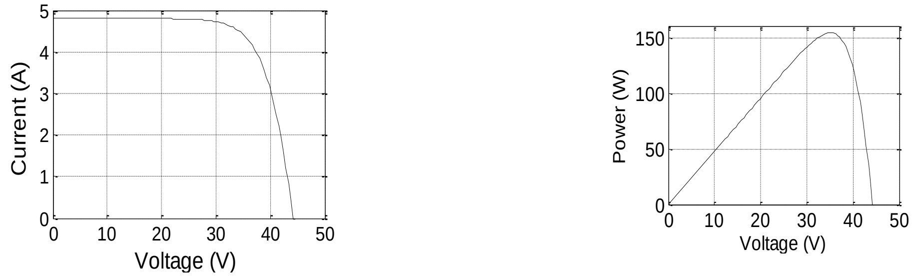

(a) (b)

Figure 4. Close up view (a) current vs voltage and (b) power vs voltage curves at T = 25°C and G=1000 W/m^2

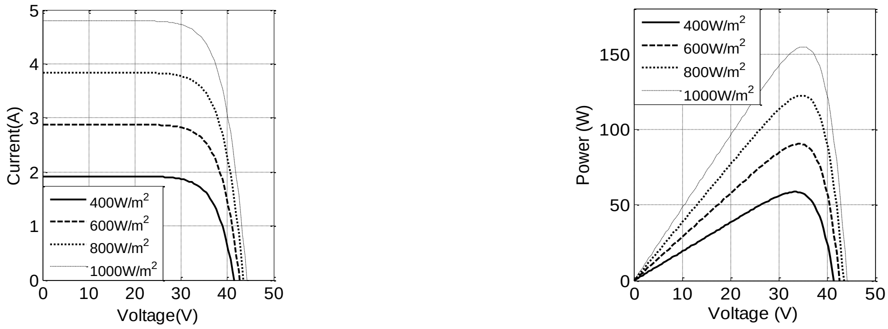

(a) (b)

Figure 5. Close up view (a) current vs voltage and (b) power vs voltage curves: effect of irradiation G

4. MODELLING OF THE DC-DC BOOST CONVERTER

A boost converter, sometimes known as a parallel chopper, is a switching power source that transforms one DC voltage to a higher-valued DC voltage. This type of converter can be used as a source-load adapter, ensuring that the power supplied by the photovoltaic generator is transferred to the MPP via control action [31], [32]. We use a step-up converter in our study, since it is the most commonly used in photovoltaic applications, particularly photovoltaic pumping systems. Different models of algorithms for searching for PPM can be found in the literature. Hill climbing, perturb & observer (P&O), and conductance increment (IncCond) are the three most widely used methods [33], [34]. The P&Q method is the most of the time used in the literature and especially in practice [35], [36].

5. MODEL MATHEMATICAL OF THREE LEVEL INVERTER

The block diagram of the proposed system is shown in Figure 6. There are three main topologies available for multi-tier inverters, namely cascaded H-bridge topology, flying capacitor topology, and neutral point or diode topology. The proposed system incorporates a neutral point topology (diode topology). The system is a voltage source inverter because the input voltage level is kept constant. The basic idea of this topology is to use diodes and generate multi-level voltages across different phases. The 3-level approach reduces the complexity of the switching circuit. There are three branches present in the system, each branch comprising four IGBT switches connected in series. Two diodes are connected on each leg in parallel to prevent activation of the wrong pair of switches [37]–[39].

5.1. Important law

It defines the state of the switch, it is worth 1 if the switch is closed and 0 if it is open, the functions of the inverter connections are related as follow [40], [41].

$$Fki = \begin{cases} 1 & \text{switch closed} \\ 0 & \text{open switch} \end{cases}$$

With k = 1, 2 or 3, represents the number of arms.

We define the function of connecting the half-arm as follows:

$$\begin{cases} F^b k1 = Fk1.Fk2 \\ F^b k0 = Fk3.Fk4 \end{cases} \quad (5)$$

denote by: 1: Half arm up; and 0: Half arm low.

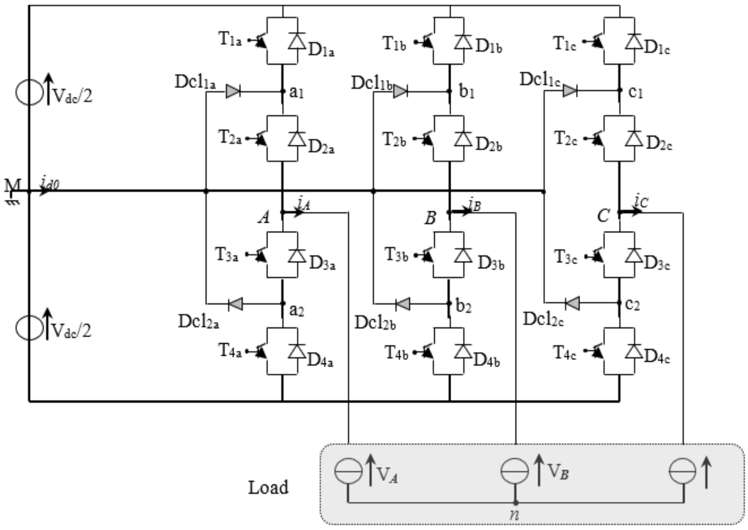

Figure 6. Three-level inverter structure NPC

The potentials of the nodes are given by the following system:

$$\begin{aligned} V_{\mathrm{AM}} &= F_{11}^{b}\frac{V_{dc}}{2} - F_{10}^{b}\frac{V_{dc}}{2} = (F_{11}^{b} - F_{10}^{b})V_{dc} \\ V_{\mathrm{BM}} &= F_{21}^{b}\frac{V_{dc}}{2} - F_{20}^{b}\frac{V_{dc}}{2} = (F_{21}^{b} - F_{20}^{b})V_{dc} \\ V_{\mathrm{CM}} &= F_{31}^{b}\frac{V_{dc}}{2} - F_{30}^{b}\frac{V_{dc}}{2} = (F_{31}^{b} - F_{30}^{b})V_{dc} \end{aligned} \quad (6)$$

The voltages are given as (7)

$$\begin{bmatrix} V_A \\ V_B \\ V_C \end{bmatrix} = \frac{1}{3}V_{\mathrm{dc}} \begin{bmatrix} 2 & -1 & -1 \\ -1 & 2 & -1 \\ -1 & -1 & 2 \end{bmatrix} \begin{bmatrix} F_{11}^{b} - F_{10}^{b} \\ F_{21}^{b} - F_{20}^{b} \\ F_{31}^{b} - F_{30}^{b} \end{bmatrix} \quad (7)$$

For currents, we can write the relation giving input currents id_1 and id_2 depending on the currents i_1, i_2 and i_3.

$$\begin{aligned} \mathrm{id}_1 &= F_{11}^{b} \cdot i_1 + F_{21}^{b} \cdot i_2 + F_{31}^{b} \cdot i_3 \\ \mathrm{id}_2 &= F_{10}^{b} \cdot i_1 + F_{20}^{b} \cdot i_2 + F_{30}^{b} \cdot i_3 \end{aligned} \quad (8)$$

i_{d0} current can be written as:

$$\mathrm{id}_0 = (i_1 + i_2 + i_3) - (F_{11}^{b} + F_{10}^{b})i_1 - (F_{21}^{b} + F_{20}^{b})i_2 - (F_{31}^{b} + F_{30}^{b})i_3 \quad (9)$$

5.2. Control triangle-sine two carriers

This strategy exploits the fact that a three-level inverter is equivalent to two inverters in series at two levels. One can use two identical carriers, out of phase by a half period from one another so as to improve the total harmonic distortion of the output voltages.

Determination of intermediate signals $V_{K.1}, V_{K.O}$.

$$\begin{cases} (V_{refK} \geq U_{P1}) \Rightarrow V_{K1} = \dfrac{V_{dc}}{2} \\ (V_{refK} < U_{P1}) \Rightarrow V_{K1} = 0 \end{cases}$$

$$\begin{cases}(V_{refK} \geq U_{P2}) \Rightarrow V_{KO} = 0\\ (V_{refK} < U_{P2}) \Rightarrow V_{KO} = -\frac{V_{dc}}{2}\end{cases}$$

6. DOUBLY FED INDUCTION MACHINE MODEL

The mathematical model of the motor supplied with voltage as a function of the state variables is given by [42]:

$$\begin{cases}\frac{d}{dt}i_{sd} = -\lambda i_{sd} + \omega_s i_{sq} + \frac{K}{T_r}\varphi_{rd} + \omega.K\varphi_{rq} + \frac{1}{\sigma L_s}v_{sd} - Kv_{rd}\\ \frac{d}{dt}i_{sq} = -\omega_s i_{sq} - \lambda i_{sq} - \omega.K\varphi_{rd} + \frac{K}{T_r}\varphi_{rq} + \frac{1}{\sigma L_s}v_{sq} - Kv_{rq}\\ \frac{d}{dt}\varphi_{rd} = \frac{L_m}{T_r}i_{sd} - \frac{1}{T_r}\varphi_{rd} + \omega.\varphi_{qr} + v_{rd}\\ \frac{d}{dt}\varphi_{rq} = \frac{L_m}{T_r}i_{sq} - \omega.\varphi_{rd} - \frac{1}{T_r}\varphi_{rq} + v_{rq}\\ \frac{d}{dt}\omega = p^2\frac{L_m}{L_r}(\varphi_{rd}i_{sq} - \varphi_{rq}i_{sd}) - \frac{f}{J}\omega - \frac{C_r}{J}\end{cases} \tag{10}$$

with:

$$T_r = \frac{L_r}{R_r}; T_s = \frac{L_s}{R_s};\ \lambda = \frac{1}{\sigma.T_r};\quad K = \frac{L_m}{\sigma L_{s.}L_r};\quad \sigma = 1 - \frac{L_m^2}{L_s L_r};\quad \omega = p.\Omega$$

The mechanical equation can be reformulated by:

$$T_{em} = \frac{p\ L_m}{L_r}(\phi_{rd}.i_{sq} - \phi_{rq}.i_{sd}) \tag{11}$$

7. ORIENTATION OF ROTOR FLUX

The orientation principle consists in aligning the rotor flux on the direct axis of the Park reference, [42], [43]. We apply:

$$\varphi_{rq} = 0, \varphi_r = \varphi_{rd} \tag{12}$$

we find:

$$T_{em} = \frac{pL_m}{L_r}(\varphi_{rd}.\,i_{sq}) \tag{13}$$

The observed flux expression found by:

$$\varphi_r = \sqrt{\varphi_{r\alpha}{}^2 + \varphi_{r\beta}{}^2}\ \text{and}\ \theta_s = tan^{-1}\left(\frac{\varphi_{r\beta}}{\varphi_{r\alpha}}\right) \tag{14}$$

– Sliding mode control design

The stator current I_{sq} is the important element for adjusting the speed of the machine.

The control law writes in this form [44], [45]:

$$I_{sq}^{ref} = I_{sq}^{eq} + I_{sq}^{n} \tag{15}$$

the machine speed setting surface is written in this expression:

$$S(\omega) = \omega_{ref} - \omega \tag{16}$$

its derivative given by:

$$\dot{S}(\omega) = \dot{\omega}_{ref} - \dot{\omega} \tag{17}$$

The expression for the speed is given by:

$$\dot{\omega} = \frac{P.L_m}{J.L_r}\left(I_{sq}.\varphi_{rd}^{ref}\right) - \frac{p}{J}C_r - \frac{f}{J}\omega \quad (18)$$

the replacement of the expression of the speed in the equation of the surface, one obtains the following equation:

$$\dot{S}(\omega) = \dot{\omega}_{ref} - \left(\frac{P.L_m}{J.L_r}\left(I_{sq}.\varphi_{rd}^{ref}\right) - \frac{p}{J}C_r - \frac{f}{J}\omega\right) \quad (19)$$

the reference current I_{sq} is replaced by $I_{sq}^{ref} = I_{sq}^{eq} + I_{sq}^{n}$, after the arrangement we find:

$$\dot{S}(\omega) = \dot{\omega}_{ref} - \left(\frac{P.L_m.\varphi_{rd}^{ref}}{J.L_r}I_{sq}^{eq} + \frac{P.L_m.\varphi_{rd}^{ref}}{J.L_r}I_{sq}^{n} - \frac{p}{J}C_r - \frac{f}{J}\omega\right) \quad (20)$$

in the two sliding and permanent modes, we find:

$$S(\omega) = 0,\ \dot{S}(\omega) = 0, I_{sq}^{n} = 0 \quad (21)$$

the equivalent command quantity I_{sq}^{eq} is written:

$$I_{sq}^{eq} = \frac{J.L_r}{P.L_m.\varphi_{rd}^{ref}}\left(\dot{\omega}_{ref} + \frac{P}{J}C_r + \frac{f}{J}\omega\right) \quad (22)$$

This condition will always be checked.

$$\dot{V}(\omega) = S(\omega).\dot{S}(\omega) < 0 \quad (23)$$

The final replacement equation is given by:

$$\dot{S}(\omega) = -\frac{P.L_m.\varphi_{rd}^{ref}}{J.L_r}I_{sq}^{n} \quad (24)$$

with $I_{sq}^{n} = K_{i_{sq}}sign(S(\omega))$

8. SYNTHESIS OF THE OBSERVER BY SLIDING MODE

The machine model equations are expressed by [46], [47]:

$$\begin{cases} \frac{d}{dt}i_{s\alpha} = -\lambda i_{s\alpha} + \omega_s i_{s\beta} + \frac{K}{T_r}\varphi_{r\alpha} + \omega.K\varphi_{r\beta} + \frac{1}{\sigma L_s}v_{s\alpha} - Kv_{r\alpha} \\ \frac{d}{dt}i_{s\beta} = -\omega_s i_{s\beta} - \lambda i_{s\beta} - \omega.K\varphi_{r\alpha} + \frac{K}{T_r}\varphi_{r\beta} + \frac{1}{\sigma L_s}v_{s\beta} - Kv_{r\beta} \\ \frac{d}{dt}\varphi_{r\alpha} = \frac{L_m}{T_r}i_{s\alpha} - \frac{1}{T_r}\varphi_{r\alpha} + \omega.\varphi_{r\beta} + v_{r\alpha} \\ \frac{d}{dt}\varphi_{r\beta} = \frac{L_m}{T_r}i_{s\beta} - \omega.\varphi_{r\alpha} - \frac{1}{T_r}\varphi_{r\beta} + v_{r\beta} \end{cases} \quad (25)$$

with:

$$T_r = \frac{L_r}{R_r}; T_s = \frac{L_s}{R_s};\ \lambda = \frac{1}{\sigma.T_r};\quad K = \frac{L_m}{\sigma L_s.L_r};\quad \sigma = 1 - \frac{L_m^2}{L_s L_r}$$

the structure of an observer is of the form:

$$\begin{cases} \dot{\hat{x}} = f(\hat{x}, u) + G_g sign(y - \hat{y}) \\ \hat{y} = h(\hat{x}) \end{cases} \quad (26)$$

were,

$\hat{x}$: Estimated state
u : Observer input or command
y and $\hat{y}$: Measured and estimated outputs, respectively.
or

$$sign(y-\hat{y}) = [sign(y_1-\hat{y}_1) \quad sign(y_2-\hat{y}_2)\ldots\ldots\ldots \; sign(y_p-\hat{y}_p)]$$

G_g : Matrix observer gain
$\hat{x}_1, \hat{x}_2, \hat{x}_3, \hat{x}_4$ the estimates of the x_1, x_2, x_3, x_4 respectively which are the state variables of $i_{s\alpha}, i_{s\beta}, \varphi_{r\alpha}, \varphi_{r\beta}$.
The observer model can be represented by [48]–[50]:

$$\begin{cases} \dot{\hat{x}}_1 = -\lambda\hat{x}_1 + \omega_s\hat{x}_2 + \frac{K}{T_r}\hat{x}_3 + \omega.K\hat{x}_4 + \frac{1}{\sigma L_s}v_{s\alpha} - Kv_{r\alpha} + g_1 I_s \\ \dot{\hat{x}}_2 = -\omega_s\hat{x}_2 - \lambda\hat{x}_2 - \omega.K\hat{x}_3 + \frac{K}{T_r}\hat{x}_4 + \frac{1}{\sigma L_s}v_{s\beta} - Kv_{r\beta} + g_2 I_s \\ \dot{\hat{x}}_3 = \frac{L_m}{T_r}\hat{x}_1 - \frac{1}{T_r}\hat{x}_3 + \omega.\hat{x}_4 + v_{r\alpha} + g_3 I_s \\ \dot{\hat{x}}_4 = \frac{L_m}{T_r}\hat{x}_2 - \omega.\hat{x}_3 - \frac{1}{T_r}\hat{x}_4 + v_{r\beta} + g_4 I_s \end{cases} \quad (27)$$

where g_1, g_2, g_3, g_4 are observer gains, $g_j = \begin{bmatrix} g_{j1} & g_{j2} \end{bmatrix}$ for $j \in \{1,2,3,4\}$.

The vector I_s is given by:

$$I_s = \begin{bmatrix} sign(S_1) \\ sign(S_2) \end{bmatrix} \quad (28)$$

with

$$S_{ob} = \begin{bmatrix} S_1 \\ S_2 \end{bmatrix} = \Gamma \begin{bmatrix} x_1-\hat{x}_1 \\ x_2-\hat{x}_2 \end{bmatrix} = \Gamma \begin{bmatrix} i_{s\alpha}-\hat{i}_{s\alpha} \\ i_{s\beta}-\hat{i}_{s\beta} \end{bmatrix}$$

and

$$\Gamma = \frac{1}{\beta(t)} \begin{bmatrix} \frac{K}{T_r} & -\omega(t)K \\ \omega(t)K & \frac{K}{T_r} \end{bmatrix} \quad (29)$$

with

$$\beta(t) = \left[\frac{K}{T_r}\right]^2 + \omega^2(t)K^2 \quad (30)$$

we take note that $e_i = x_j - \hat{x}_j$ for $j \in \{1,2,3,4\}$.

$$\begin{aligned} \dot{e}_1 &= \frac{K}{T_r}e_3 + \omega K e_4 - g_1 I_s \\ \dot{e}_2 &= \frac{K}{T_r}e_4 - \omega K e_3 - g_2 I_s \\ \dot{e}_3 &= -\frac{1}{T_r}e_3 - \omega e_4 - g_3 I_s \\ \dot{e}_4 &= -\frac{1}{T_r}e_4 + \omega e_3 - g_4 I_s \end{aligned} \quad (31)$$

The stability study results in obtaining the gains g1 and g2 to have $S_{ob} = 0$.
The gains g_3 and g_4 are obtained when $S_{ob} \equiv \dot{S} \equiv 0$is locally stable.

The state variables x3(t) and x4(t) are limited and let us examine then the system (31) is given by:

$$[g_1 \quad g_2] = \begin{bmatrix} g_{11} & g_{12} \\ g_{21} & g_{22} \end{bmatrix} = \Gamma^{-1}\Delta, \quad \Delta = \begin{bmatrix} \delta_1 & 0 \\ 0 & \delta_2 \end{bmatrix}$$

$$\begin{bmatrix} g_{31} & g_{32} \\ g_{41} & g_{42} \end{bmatrix} = \begin{bmatrix} \left(q_1 - \frac{1}{T_r}\right)\delta_1 & -\omega(t)\delta_2 \\ \omega(t)\delta_1 & \left(q_2 - \frac{1}{T_r}\right)\delta_2 \end{bmatrix} \tag{32}$$

were

$$\begin{cases} \delta_1 > \rho_3 + \left|\hat{\phi}_{r\alpha}\right| + a_{\max}\left|e_1\right| + b_{\max}\left|e_2\right| \\ \delta_2 > \rho_4 + \left|\hat{\phi}_{r\beta}\right| + b_{\max}\left|e_1\right| + a_{\max}\left|e_2\right| \end{cases}$$

with

$$a r^2{}_{1}{}_{2_{max}},\ b\ \ {}^{2}_{r}{}_{2}\left(\frac{1}{K} + 2p^2\eta_1^2\right)_{max}$$
$$|x_3(t)| \le \rho_3,\ |x_4(t)| \le \rho_4,\ q_1 q_2 > 0$$

$S_{\text{ob}} \equiv \dot{S} \equiv 0$ this condition is fulfilled, then we get:

$$\begin{cases} \dot{e}_3 = -q_1 e_3 \\ \dot{e}_4 = -q_2 e_4 \end{cases} \tag{33}$$

where q_1, q_2 >0 this achieves the stability of e_3 and e_4.

– Sliding mode observer for motor speed estimation

The (30) can be rewritten as follows [48], [49], [50]:

$$\dot{e}(\omega) = A(\omega).e + C_g(\omega).I_{sg}(\omega) \tag{34}$$

with

$$\dot{e}(\omega) = \begin{bmatrix} \dot{e}_1 \\ \dot{e}_2 \\ \dot{e}_3 \\ \dot{e}_4 \end{bmatrix};\ A(\omega) = \begin{bmatrix} 0 & 0 & \frac{K}{T_r} & K.\omega \\ 0 & 0 & -K.\omega & \frac{K}{T_r} \\ 0 & 0 & \frac{-1}{T_r} & -\omega \\ 0 & 0 & \omega & \frac{-1}{T_r} \end{bmatrix};\ G_g(\omega) = \begin{bmatrix} \frac{K}{T_r}.\delta_1 & \frac{K}{T_r}.\omega.\delta_2 \\ -\frac{K}{T_r}.\omega.\delta_1 & \frac{K}{T_r}.\delta_2 \\ \left(q_1 - \frac{1}{T_r}\right).\delta_1 & -\omega.\delta_2 \\ \omega.\delta_1 & \left(q_2 - \frac{1}{T_r}\right).\delta_2 \end{bmatrix}$$

the motor speed is replaced by its estimated magnitude $\hat{\omega} = \omega - \Delta\omega$, the system (33) becomes:

$$\dot{e}(\hat{\omega}) = A(\hat{\omega}).e + G_g(\hat{\omega}).I_{sg}(\hat{\omega}) \tag{35}$$

with

$$A(\hat{\omega}) = A(\omega) + \Delta\Omega \tag{36}$$

$$G_g(\hat{\omega}) = G_g(\omega) + \Delta G_g \tag{37}$$

$$I_{sg} = sign\begin{bmatrix} S_1 + \frac{\frac{K}{T_r}.e_2.\Delta\omega}{\beta} \\ S_2 + \frac{\frac{K}{T_r}.e_1.\Delta\omega}{\beta} \end{bmatrix} \tag{38}$$

and

$$\Delta A = \begin{bmatrix} 0 & 0 & 0 & -K.\Delta\omega \\ 0 & 0 & K.\Delta\omega & 0 \\ 0 & 0 & 0 & \Delta\omega \\ 0 & 0 & -\Delta\omega & 0 \end{bmatrix};\ \Delta G_g = \begin{bmatrix} 0 & \frac{K}{T_r}.\Delta\omega.\delta_2 \\ -\frac{K}{T_r}.\Delta\omega.\delta_1 & 0 \\ 0 & \Delta\omega.\delta_2 \\ -\Delta\omega.\delta_1 & 0 \end{bmatrix}$$

the applied Lyapunov function is given by:

$$v = \frac{1}{2} e.e^T + \frac{1}{2\lambda}(\Delta\omega)^2 \quad (39)$$

we derive the (38) we find:

$$\dot{v} = e^T.\dot{e}(\widehat{\omega}) + \frac{1}{\lambda}\Delta\omega.\dot{\widehat{\omega}} \quad (40)$$

we replace the expression of $\dot{e}(\hat{\omega})$ in the (39), it comes:

$$\dot{v} = e^T\{(A(\omega) + \Delta A).e - (G_g + \Delta G_g).I_{sg}(\omega)\} + e^T.G_g.I_{sg} - e^T.G_g.I_{sg} + \frac{1}{\lambda}\Delta\omega.\dot{\widehat{\omega}} \quad (41)$$

after arrangement we get:

$$\dot{v} = e^T\left[\left(A(\omega)e - G_g.I_{sg}(\omega)\right) + \left(G_g.I_{sg}(\omega) - (G_g + \Delta G_g).I_{sg}(\omega)\right)\right] + \frac{1}{\lambda}\Delta\omega.\dot{\widehat{\omega}} + e^T.\Delta A.e \quad (42)$$

with

$$e^T.\Delta A.e = \Delta\omega.\{p.K.(e_1.\hat{x}_4 - e_2.\hat{x}_3)\} + p.K.\Delta\omega(e_2.x_3 - e_1.x_4) \quad (43)$$

based on this equality:

$$\frac{1}{\lambda}\Delta\omega.\dot{\hat{\omega}} + \Delta\omega.\{p.K.(e_1.\hat{x}_4 - e_2.\hat{x}_3)\} = 0 \quad (44)$$

we have $\Delta\omega \neq 0$, motor speed adaptation law given by this expression:

$$\dot{\widehat{\omega}} = \lambda.K.p.(e_1.\hat{x}_4 - e_2.\hat{x}_3) \quad (45)$$

$$\dot{\widehat{\omega}} = \lambda.K.p.\left((i_{s\alpha} - \hat{\imath}_{s\alpha}).\hat{\varphi}_{r\beta} - \left(i_{s\beta} - \hat{\imath}_{s\beta}\right).\hat{\varphi}_{r\alpha}\right) \quad (46)$$

in (33) then becomes:

$$\dot{v} = e^T.e + e^T.\{G_g.I_{sg}(\widehat{\omega}) - (G_g + \Delta G_g).I_{sg}(\widehat{\omega})\} + p.K.\Delta\omega.(e_2.x_3 - e_1.x_4) \quad (47)$$

If the (48) is satisfied, the system can be said to be stable:

$$e^T.\{G_g.I_{sg}(\widehat{\omega}) - (G_g + \Delta G_g).I_{sg}(\widehat{\omega})\} + p.K.\Delta\omega.(e_2.x_3 - e_1.x_4) < 0 \quad (48)$$

this result defines the stability.

9. INTERPRETATION OF SIMULATION RESULTS

To check the results of the sensorless vector control of this machine, we carried out a series of tests such as variation of the load torque with continuation of the speed and inversion of the direction of rotation. Figure 7 represents a three-phase machine powered by two PWM voltage inverters, one at the stator level and the other at the rotor level, these two inverters are powered by a photovoltaic chain, a controller speed robustness and for the estimation of the fluxes, the stator currents and the rotational speed we used a sliding mode observer. The parameters of the 1.5 MW machine are shown in the list: 1.5 Kw, 1,450 rpm, 50 Hz, R_r=1.68 Ω, R_s=1.75Ω, L_s=295 mH, L_r=104 mH, L_m=165 mH, J=0.01 kg.m^2, *f*=0.0027 kg.m^2/s.

The proposed strategy is presented in Figure 8. Figure 9 (see Appendix) shows the results of an off-load start of a motor with a reference speed of 250 rad/s, and the effect of applying a load torque of value Tr=10 Nm to the time t =1.5s and its subsequent elimination at time t=2.5s

We observe that:

– The evaluation of the rotation speed is almost impeccable shown in Figure 9(a).

– The desired speed absolutely follows the existing speed with a static error equal to zero shown in Figure 9(b)
– Better susceptibility to large imbalances with a short rejection time, thanks to the use of a strong and robust control loop by the sliding mode controller. The line current is perfectly sinusoidal shown in Figure 9(c) and Figure 9(d).
– In addition, an excellent orientation of the rotor flux is observed on the direct axis shown Figure 9(g). This has enormous repercussions on the electromagnetic torque shown in Figure 9(e). During changes in the setpoints, and in particular during the reversal of rotation, the change in the direction of the torque does not degrade the orientation of the flux.

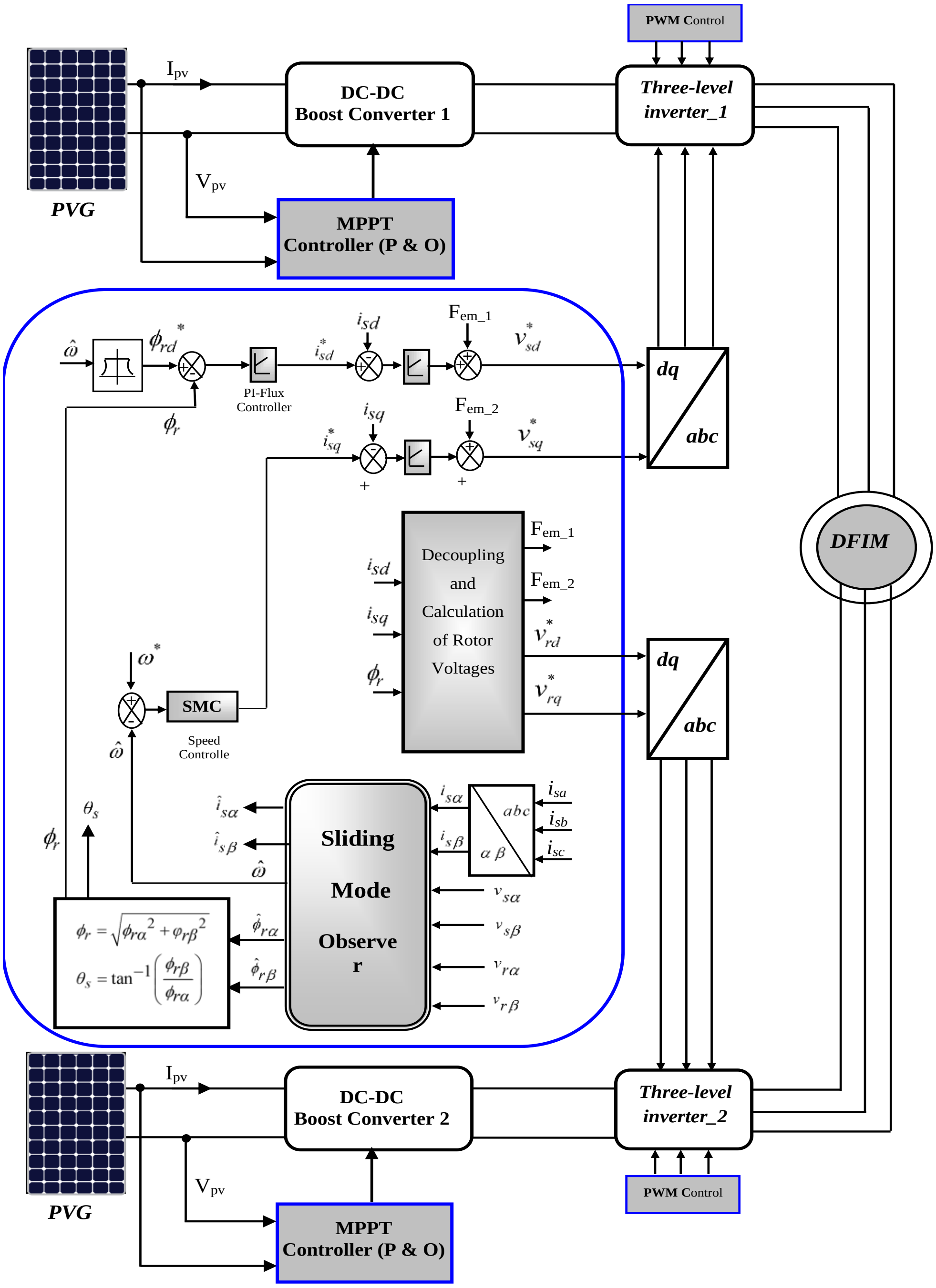

Figure 7. Schematic of dual-feed motor sensorless vector control using a sliding mode observer fed by photovoltaic solar panel

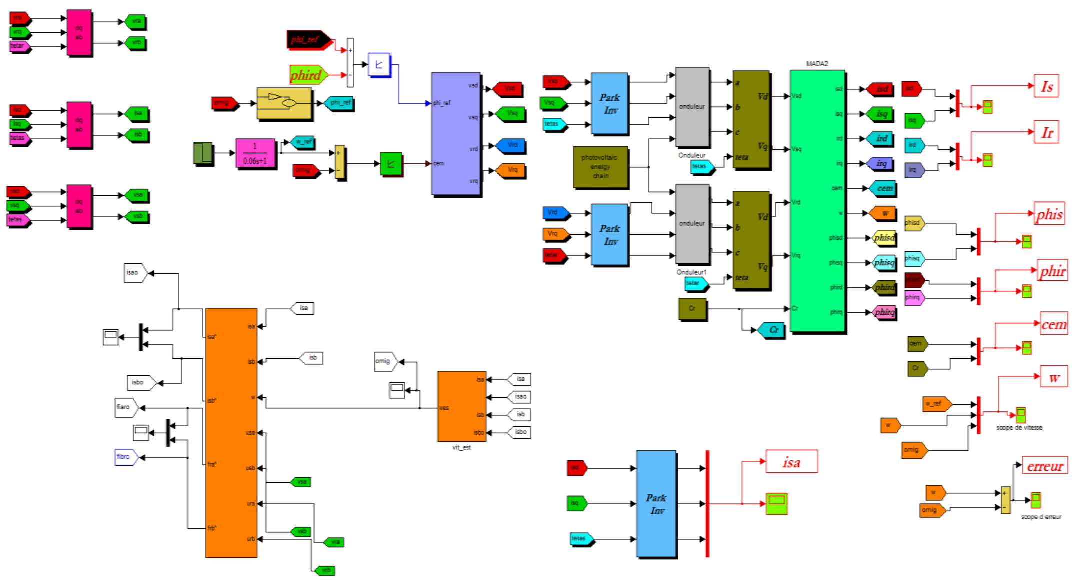

Figure 8. The Simulink model of strategy proposed

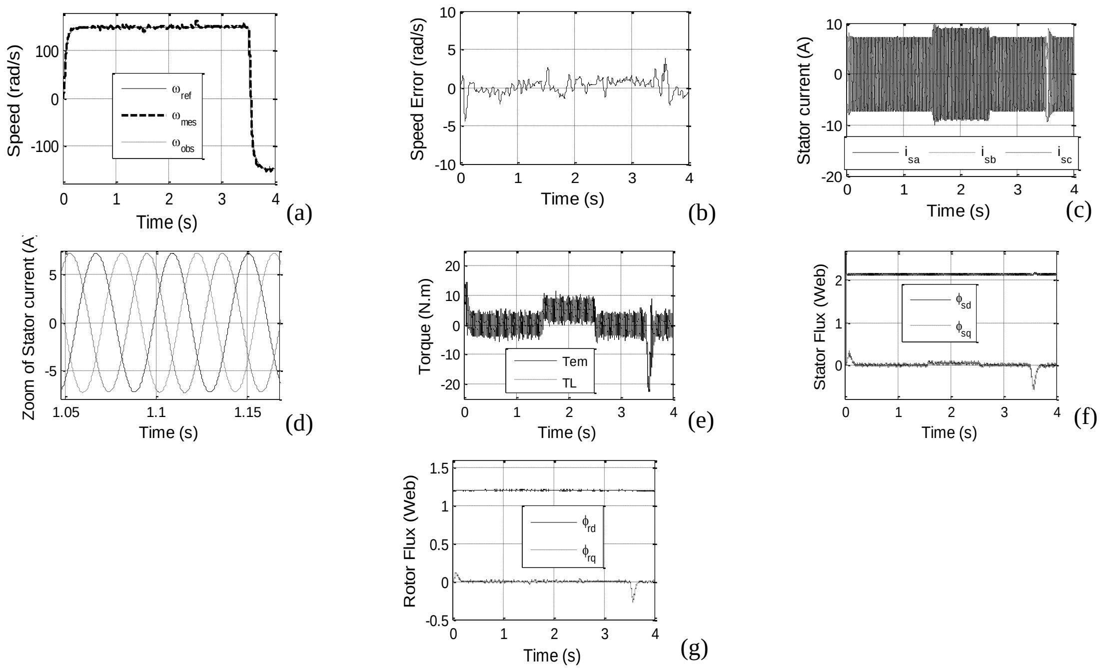

Figure 9. Close up view Solar PV powered system responses with MPPT (a) motor speed, (b) error speed, (c) stator current, (d) zoom of stator current, (e) electromagnetic torque, (f) stator flux, and (g) rotor flux

10. CONCLUSION

The results obtained clearly show the efficiency and usefulness of the MPPT algorithm for operating the system under optimal conditions, by maintaining the power at its maximum value at each irradiation value, whatever the climatic conditions, these results also prove that observer by sliding mode using an algorithm based on the stability criterion of lyapunov in the estimation of the speed, allowed us to have a good estimate of the flux and the speed of rotation of the motor.

REFERENCES

[1] S. S. Bohra, "DC-current sensor-less MPPT based grid-fed single-phase photovoltaic (PV) micro-inverter," *Applied Solar Energy*, vol. 56, no. 2, pp. 85–93, 2020, doi: 10.3103/S0003701X20020036.

[2] M. A. G. de Brito, L. Galotto, L. P. Sampaio, G. d. A. e Melo, and C. A. Canesin, “Evaluation of the main MPPT techniques for photovoltaic applications,” *IEEE Transactions on Industrial Electronics*, vol. 60, no. 3, pp. 1156-1167, March 2013, doi: 10.1109/TIE.2012.2198036.

[3] K. Bhargav, and A. S. M. Antony, “MPPT controller based solar power generation using a multilevel inverter,” *International Journal of Engineering and Technology (IJET)*, vol .8 no. 1, Feb-Mar 2016.

[4] Y. Guo, and Y. Xiang, “Cost–benefit analysis of photovoltaic-storage investment in integrated energy systems,” *Energy Reports*., vol. 8, no. 3, August 2022, pp. 66–71, doi: 10.1016/j.egyr.2022.02.158.

[5] C. Manjunath, J. Reddy, K. Sai Ranjith Reddy, I.R. Ganesh Kumar, and S. Sanket, “Energy, exergy performance and analysis of 50w solar photovoltaic module,” *Materials Today: Proceedings*., vol. 54, pp. 531–536, January 2022, doi: 10.1016/j.matpr.2021.12.209.

[6] H. Alami Aroussi, E. Ziani, M. Bouderbala, and B. Bossoufi, “Improvement of direct torque control applied to doubly fed induction motor under variable speed,” *International Journal of Power Electronics and Drive System (IJPEDS)*, vol. 11, no. 1, pp. 97–106, March 2020, doi: 10.11591/ijpeds.v11.i1.pp97-106.

[7] Dj. Cherifi, and Y. Miloud, “Performance analysis of adaptive fuzzy sliding mode for nonlinear control of the doubly fed induction motor,” *Indonesian Journal of Electrical Engineering and Informatics (IJEEI)*, vol. 6, no. 4, pp. 436-447, December 2018, doi: 10.52549/ijeei.v6i4.605.

[8] N.El Ouanjli, A. Derouich, A. El Ghziza, Y. El Mourabit, B. Bossoufi, and M.Taoussi., “Contribution to the performance improvement of doubly fed induction machine functioning in motor mode by the DTC control,” *International Journal of Power Electronics and Drive Systems (IJPEDS)*, vol. 8, no. 3, pp. 1117–1127, September 2017.

[9] A. Zemmit, S. Messalti, and A. Harrag, “A new improved DTC of doubly fed induction machine using GA-based PI controller,” *Ain Shams Eng. J.*, vol. 9, no. 4, pp. 1877–1885, December 2018, doi: 10.1016/j.asej.2016.10.011.

[10] M. Zerzeri, and A. Kheder, “Optimal speed–torque control of doubly-fed induction motors: Analytical and graphical analysis,” *Computers and Electrical Engineering*, vol. 93, July 2021, doi: 10.1016/j.compeleceng.2021.107258.

[11] A. Herizi, A. Bouguerra, S. Zeghlache, and R. Rouabhi, “Backstepping control of a doubly-fed induction machine based on fuzzy controller,” *European Journal of Electrical Engineering*, vol. 20, no. 5-6, pp. 645–657, 2018, doi: 10.3166/EJEE.20.645-657.

[12] B. Kirankumar, Y.V. Siva Reddy, and M. Vijayakumar, “Multilevel inverter with space vectormodulation: intelligence direct torque controlof induction motor,” *IET Power Electron.*, vol. 10, no. 10, pp. 1129–1137, 2017, doi: 10.1049/iet-pel.2016.0287.

[13] N. El Ouanjli, S. Motahhir, A. Derouich, A. El Ghzizal, A. Chebabhi, and M. Taoussi, “Improved DTC strategy of doubly fed induction motor using fuzzy logic controller”, *Energy Reports*, vol. 5, pp. 271–279, 2019, doi: 10.1016/j.egyr.2019.02.001.

[14] C. Belfedal, S. Gherbi, M. Sedraoui, S. Moreaua, G. Champenois, T. Allaoui, and M.A. Denaï, “Robust control of doubly fed induction generator for stand-alone applications,” *Electric Power Systems Research*, vol. 80, no. 2, pp. 230–239, February 2010, doi: 10.1016/j.epsr.2009.09.002.

[15] Y. Sahri *et al*., “Advanced fuzzy 12 DTC control of doubly fed induction generator for optimal power extraction in wind turbine system under random wind conditions,” *Sustainability.*, vol. 13, no. 11593, 2021, doi: 10.3390/su132111593.

[16] A. Tiwari, B. Kumar, and Y. K. Chauhan, “ANN based RF-MRAS speed estimation of induction motor drive at low speed,” 2017 *International conference of Electronics, Communication and Aerospace Technology (ICECA)*, doi: 10.1109/ICECA.2017.8212789.

[17] A. Ammar, A. Kheldoun, B. Metidji, T. Ameid, and Y.Azzoug, “Feedback linearization based sensorless direct torque control using stator flux MRAS-sliding mode observer for induction motor drive,” *ISA Transactions*, vol. 98, pp. 382–392, March 2020, doi: 10.1016/j.isatra.2019.08.061.

[18] M. Elgohary, E. Gouda, and S. S. Eskander, “Intelligent control of induction motor without speed sensor,” *International Journal of Power Electronics and Drive Systems (IJPEDS)*, vol. 12, no. 2, pp. 715–725, Jun 2021, doi: 10.11591/ijpeds.v12.i2.pp715-725.

[19] L. Yuan, H. Feng-you, and Y. Zong-bin, “Study on sliding mode speed control with RBF network approach for doubly-fed induction motor,” *International Conference on Intelligent Human-Machine Systems and Cybernetics*, 2009 IEEE, doi: 10.1109/IHMSC.2009.208.

[20] O. Moussa, R. Abdessemed, S.Benaggoune, and H. Benguesmia, “ Sliding mode control of a grid-connected brushless doubly fed induction generator,” *European Journal of Electrical Engineering*, vol. 21, no. 5, pp. 421–430, October 2019, doi: 10.18280/ejee.210504.

[21] M. Benmeziane, S. Zebirate, A. Chaker, and Z. Boudjema, “Fuzzy sliding mode control of doubly-fed induction generator driven by wind turbine”, *International Journal of Power Electronics and Drive System (IJPEDS)*, vol. 10, no. 3, pp. 1592–1602, Sep 2019, doi: 10.11591/ijpeds.v10.i3.pp1592-1602.

[22] G. D. Prasad, V. Jegathesan, and V. Moorthy, “Minimization of power loss in newfangled cascaded H-bridge multilevel inverter using in-phase disposition PWM and wavelet transform based fault diagnosis,” *Ain Shams Engineering Journal*, vol. 9, no. 4, pp. 1381–1396, 2018, doi: 10.1016/j.asej.2016.09.008.

[23] M. Hammami, G. Rizzoli, R. Mandrioli, and G. Grand, “Capacitors voltage switching ripple in three-phase three-level neutral point clamped inverters with self-balancing carrier-based modulation,” vol. 11, no. 12, 2018, doi: 10.3390/en11123244.

[24] S. Necaibia, MS. Kelaiaia, H.Labar, A. Necaibia, and E. Castronuovo, “ Enhanced auto-scaling incremental conductance MPPT method, implemented on low-cost microcontroller and SEPIC converter,” *Solar Energy*, vol. 180, pp. 152–168, 2019, doi: 10.1016/j.solener.2019.01.028.

[25] S. Raj, and R. Kumar, “A reinvigorated strategy for the analysis of optimal parameters for modeling of Solar Photovoltaic modules under variable conditions,” *Energy Reports*., vol. 7, pp. 5965–5976, Novembre 2021, doi: 10.1016/j.egyr.2021.08.189.

[26] K. Yaman, and G. Arslan, “A detailed mathematical model and experimental validation for coupled thermal and electrical performance of a photovoltaic (PV) module,” *Applied Thermal Engineering*., vol. 195, August 2021, doi: 10.1016/j.applthermaleng.2021.117224.

[27] N. Aouna, and N. Bailek, “Evaluation of mathematical methods to characterize the electrical parameters of photovoltaic modules,” *Energy Conversion and Management.*, vol. 193, pp. 25–38, August 2019, doi: 10.1016/j.enconman.2019.04.057.

[28] A. Asbayou *et al*., “Method using simple RLC circuit for electrical characterization of PV panels,” *Materials Today: Proceedings.*, vol. 58, 17 January 2022, pp. 1033-1038, doi: 10.1016/j.matpr.2022.01.034.

[29] C. Bertrand, C. Housmans, J. Leloux, and M. Journee, “Solar irradiation from the energy production of residential PV systems,” *Renewable Energy*, vol. 125, pp. 306–318, September 2018, doi: 10.1016/j.renene.2018.02.036.

[30] M. Das, and R. Manda, “Effect of solar radiation and operating factor of the PV module on the loss of load probability of a PV-Battery system,” *Materials Today: Proceedings*, vol. 56, pp. 2767–2773, 2022, doi: 10.1016/j.matpr.2021.10.010.

[31] A. Raj, S. Raj Arya, and J. Gupta, “Solar PV array-based DC–DC converter with MPPT for low power applications,” *Renewable Energy Focus*, vol. 34, pp. 109–119, September 2020, doi: 10.1016/j.ref.2020.05.003.

[32] P. V. Nandankar, P. P. Bedekar, and P. V. Dhawas, “Efficient DC-DC converter with optimized switching control: A comprehensive review,” *Sustainable Energy Technologies and Assessments*, vol. 48, December 2021, doi: 10.1016/j.seta.2021.101670.

[33] Z. Hu, H. Norouzi, M. Jiang, S. Dadfar, and T. Kashiwagi, “Novel hybrid modified krill herd algorithm and fuzzy controller based MPPT to optimally tune the member functions for PV system in the three-phase grid-connected mode,” *ISA Transactions*, vol. 129,

pp. 214–229, 2022, doi: 10.1016/j.isatra.2022.02.009 .
[34] A. I. M. Ali, and H. R. A. Mohamed, "Improved P&O MPPT algorithm with efficient open-circuit voltage estimation for two-stage grid-integrated PV system under realistic solar radiation," *International Journal of Electrical Power and Energy Systems*, vol. 137, May 2022, doi: 10.1016/j.ijepes.2021.107805.
[35] K. Ishaque, Z. Salam, H. Taheri, and A. Shamsudin, "Maximum power point tracking for PV system under partial shading condition via particle swarm optimization," *2011 IEEE Applied Power Electronics Colloquium (IAPEC)*, 2011, pp. 5-9. doi: 10.1109/IAPEC.2011.5779866 .
[36] Y. Shaiek, M. B. Smida, A. Sakly, and M. F. Mimouni, "Comparison between conventional methods and GA approach for MPPT of solar PV generators," *Solar Energy*, vol. 90, pp. 107–122, April 2013, doi: 10.1016/j.solener.2013.01.005.
[37] I. Ouerdani, H. Ben Abdelghani, A. Bennani Ben Abdelghani, D. Montesinos-Miracle, and I. Slama-Belkhodja, "Space vector modulation technique for 3-level NPC converter with constant switching frequency," *Hindawi publishing corporation, Advances in power Electronis*, vol. 2016, 2016, doi: 10.1155/2016/6478751.
[38] H.-C. In, S.-M. Kim, and K.-B. Lee, "Design and control of small DC-Link capacitor-based three-level inverter with neutral-point voltage balancing," *Energies*, vol. 11, no. 6, 2018, doi: 10.1109/IAPEC.2011.5779866.
[39] K. Cherifi, Y. Miloud, and M. Mostefai, "A modified multilevel inverter topology with maximum power point tracking for photovoltaic systems," *Journal of Engineering Science and Technology*., vol. 14, no. 1, pp. 351–369, 2019.
[40] C. Wang, Z. Li, and H. Xin, "Neutral-point voltage balancing strategy for Three-level converter based on disassembly of zero level," *Journal of Power Electronics*, vol. 19, no. 1, pp. 79–88, January 2019, doi: 10.6113/JPE.2019.19.1.79.
[41] A. Ventosa-Cutillas, P. Montero-Robina, F. Umbría, F. Cuesta, and F. Gordillo, "Integrated control and modulation for three-level NPC rectifiers," *Energies,* vol. 12, no. 9, April 2019, doi: 10.3390/en 12091641.
[42] S. K. Samal, S. Jena, B. P. Ganthia, S. Kaliappan, M. Sudhakar, and S. K. Sriram Kalyan, "Sensorless speed contorl of doubly-fed induction machine using reactive power based MRAS," *Journal of Physics: Conference Series,* 2022, vol. 21-61, doi: 10.1088/1742-6596/2161/1/012069.
[43] F. Wang, Z. Zhang, X. Mei, J. Rodríguez, and R. Kennel, "Advanced control strategies of induction machine: field oriented control, direct torque control and model predictive control," *Energies*, vol. 11, no. 1, January 2018, doi: 10.3390/en11010120.
[44] S. Abderazak, and N. Farid, "Comparative study between Sliding mode controller and Fuzzy Sliding mode controller in a speed control for doubly fed induction motor", *(CEIT-2016) Tunisia, Hammamet- December, 16-18, 2016.* doi: 10.1109/CEIT.2016.7929044.
[45] Y. Bekakra, D. Ben Attous, Z. Tir, and O. Malik, "Improvement in speed performance of an induction motor with sliding mode controller and ann for DTC," *Journal of Fundamental and Applied Sciences*., vol. 12, no. 1, pp. 86–114, January 2020.
[46] Q. Wang, M. Tan, and S. Yang, "A novel sliding-mode observer for doubly-fed induction generator," *Applied Mechanics and Materials*, vol. 511-512, pp. 1105-1109, 2014, doi: 10.4028/www.scientific.net/AMM.511-512.1105.
[47] Qinglong WANG, Shuying Yang, "Sensorless Control of Doubly-fed Induction Generator Based on Adaptive Sliding-mode Observer", *Advanced Materials Research*, vols. 860-863, pp. 337-341, 2014, doi: 10.4028/scientific.net/AMR.860-863.337.
[48] L. Zhang, Z. Dong, L. Zhao, and S. Laghrouche, "Sliding mode observer for speed sensorless linear induction motor drives," *IEEE Access*, vol. 9, 2021, doi: 10.1109/ACCESS.2021.3067805.
[49] C. Djamila and Y. Miloud, "High performance of sensorless sliding mode control of doubly fed induction motor associated with two multilevel inverters fed by VFDPC_SVM rectifier," *Indonesian Journal of Electrical Engineering and Informatics (IJEEI)*, vol. 8, no. 2, June 2020, pp. 242-255, doi: 10.52549/ijeei.v8i2.1481.
[50] K. Negadi, A. Mansouri, B. Khtemi, "Real time implementation of adaptive sliding mode observer based speed sensorless vector control of induction motor," *Serbian Journal of Electrical Engineering*, vol. 7, no. 2, pp. 167–184, November 2010, doi: 10.2298/SJEE1002167N.

BIOGRAPHIES OF AUTHORS

Mekki Mounira has been the research professor at the university of Oum El Bouaghi in the east of Algeria since 2015 in the Electrical engineering department. She got the PhD degree in Electrical Engineering at Annaba University of Algeria in 2014. Her research interests include renewables energies, power electronics, power quality and stability and dynamics of electrical networks. She can be contacted at email: mouniramekki9@gmail.com.

Cherifi Djamila was born in Algeria. She received her Engineer and Ms degrees in Electrical Engineering in 2005 and 2008, respectively. She received her PhD in Electrical Engineering in 2014 from USTO in Algeria. She is currently research professor in the department of Electrical Engineering at the university of Saida, Algeria. Her current areas of research include design and sensorless control of doubly feed AC machines, power electronics and renewable energy. She can be contacted at email: d_cherifi@yahoo.fr.